Renewable Energy 200 (2022) 37–47

Contents lists available at ScienceDirect

Renewable Energy

journal homepage: www.elsevier.com/locate/renene

Energy assessment of potential locations for OWC instalation at the Portuguese coast

Gael Anastas [a,*], João Alfredo Santos [b,c], C.J.E.M. Fortes [a], Liliana V. Pinheiro [a]

[a] Laboratório Nacional de Engenharia Civil, Avenida do Brasil, 101, 1700-066, Lisboa, Portugal
[b] ISEL – Instituto Superior de Engenharia de Lisboa, Instituto Politécnico de Lisboa, Rua do Conselheiro, Emídio Navarro, 1, 1959-007, Lisboa, Portugal
[c] CENTEC – Centre for Marine Technology and Ocean Engineering, Instituto Superior Técnico, Avenida Rovisco Pais, 1, 1049-001, Lisboa, Portugal

ARTICLE INFO

Keywords:
Wave energy converter
Oscillating water column
SWAN
Exploitable energy

ABSTRACT

This work aims to determine the exploitable wave energy resource at five potential sites close to harbour protection facilities at the Portuguese coast, namely at the Azores archipelago, at Madeira Island and at Sines, on the coast of mainland Portugal. For that purpose, a third-generation wave model SWAN is used to transfer the offshore estimates of sea wave conditions to those points over the last 40 years. Sea states and wind fields are provided by the climate reanalysis datasets ERA5. Using sea states as boundary conditions and wind fields as forcings in the numerical domains of the SWAN model, the sea states were propagated shoreward, in order to estimate and analyse the wave conditions in the regions of interest. By combining the average energy flux per unit length of wave front and the probability of occurrence of each sea state, the average exploitable annual energy per unit length of wave crest can be computed. The variability of this energy flux is analysed since it is of paramount importance for the efficiency of Wave Energy Converters (WEC). This assessment showed that the best location for the installation of dual-chamber OWC devices is at the Azores archipelago.

1. Introduction

The increased need for renewable energy resources in the recent decades has resulted in a significant growth in the research and development of Wave Energy Converters (WEC) with the goal of meeting the escalating demand for clean and renewable energies. Because of its predictability, seasonal stability, low aesthetic impact, and overall high energy carried by ocean waves [1], the possibilities for this energy exploitation exceed those of wind or solar energy for electrical production. Wave energy is not only more predictable than wind or solar energy, but it also has a higher energetic density, which allows more energy to be extracted in smaller regions. Moreover, the relevance of installing such energy extraction systems in island environments is heightened by the fact that they can help local communities achieve energy autonomy.

The exploitation of the wave energy resource can be achieved thanks to a broad range of technological solutions, which are reported in the following comprehensive reviews: Drew et al. [2], Falcão [3], Falnes [4]. The present study focuses on a fixed Oscillating Water Column (OWC) incorporated in the trunk of a breakwater. The design and construction of the structure are the most critical issues (not considering the air turbine technology) in terms of efficiency, environmental impact, and financial viability for the OWC technology.

Most WEC have been conceived as offshore devices, where the highest wave energy densities are found. The installation of WEC in the nearshore has been ignored in the past due to lower gross energy densities, without considering the differences in characteristics between offshore and nearshore wave energy resources. However, a simple scaling of the wave climate inadequately describes the nearshore wave climate. A better representation is required to correctly assess the nearshore wave energy resource potential. The integration of the plant structure into a breakwater has several advantages, including shared construction costs, access for operation and maintenance, and no additional environmental impact.

Since these fixtures are not omni-directional and installed in fixed positions, it can be easily understood that the amount of energy exploitable by a given device is influenced by its own orientation and the relative incident wave directions [5]. Therefore, wave directions must be considered in the wave energy flux estimation to ensure a proper assessment. Such an approach was successfully applied by the Electric Power Research Institute Group to determine the available and recoverable wave energy resource on the United States coastline [6].

* Corresponding author.
E-mail addresses: ganastas@lnec.pt (G. Anastas), jasantos@dec.isel.ipl.pt (J. Alfredo Santos), jfortes@lnec.pt (C.J.E.M. Fortes), lpinheiro@lnec.pt (L.V. Pinheiro).

https://doi.org/10.1016/j.renene.2022.09.082
Received 23 November 2021; Received in revised form 1 September 2022; Accepted 19 September 2022
Available online 27 September 2022

Accordingly, a numerical model setup was built to estimate the wave climate at five locations along the Portuguese coast, and the performance of the numerical model is assessed by comparing its results to on-site measurements.

Similar works were already performed, as described in Rusu et al. [7], where a WAM and SWAN model of the Madeira Island surroundings are set-up, concluding on the high energetic potential of this area and underlying the sensibility of SWAN model to diffraction and triad non-linear interaction. Other examples focus on the Azores Islands region as in Matos et al. [8] where the study time frame is 10 years, and the data were provided by the ECMWF ERA4 dataset. Also, Rusu & Guedes [9] assess the numerical model accuracy against GFO satellite altimeter data and point out the presence of energy hotspots and highlight the low variability of the incoming wave direction in the archipelago area. Furthermore, the studies described in Rusu & Soares [10] and in Mota & Pinto [11], focused on the Portuguese mainland coast, do identify the central part of Portuguese west coast as the most suitable for WEC and emphasize the importance of the coastline orientation in the energy losses due to wave refraction. In Rusu [12], the theoretical available power is estimated for different device technologies and coastal environments. It concludes on the importance of combining the power matrix of each device with the wave state distribution in the area of interest so as to optimize the considered WEC device technology. In all those works, the wind field data were provided by the HIPOCAS project. Comparable methodologies were followed at other locations worldwide: Iglesias & Carballo [13] focused on the Canary Islands region, Bento et al. [14] considered the north coast of Spain, and Monteforte et al. [15] contemplated the Sicilian nearshore. In Gonçalves et al. [16], both third-generation wave model WAVEWATCH III and SWAN are used to assess the available energy in the Canary Islands focusing on its seasonal variability and predictability. Ahn et al. [17] built a 30-year WaveWatch III model for coastal waters of the United States introducing the inter-annual variability as a relevant capacity factor. A wave energy assessment of the Indonesian sea is performed in Ribal et al. [18] based on a nested downscaled model and concluding on the high potential for WEC installation in that region. Recently, Patel et al. [19], established a wind and wave energy assessment along the Indian coast. They introduced a co-location feasibility index that can be an instructive base to allow the development of combined energy exploitation.

Five potential locations along the Portuguese coasts were preselected for OWC installation based on the aforementioned works conclusions and the existing facilities potential. The present work aims to refine the previous research outcomes providing accurate parameters for OWC WEC installation site evaluation. It considers a much longer time frame than the previous works and introduces the concept of exploitable energy for this specific WEC technology [5]. It also uses the data provided by the new ECMWF ERA5 reanalysis dataset for both wind fields and sea-wave inputs, whose reliability has been demonstrated in Anastas et al. [20]. Both variability and survival criteria are studied. Ultimately, it provides an accurate description of the available energy at each location and the tools to select the most suitable site considering the device technological and physical constraints.

2. Oscillating water column concept

For decades it has been ascertained that the energy carried by oscillatory ocean waves can be used to drive devices that convert it into clean electric energy. Depending on their type, design, and location with respect to the coast, a great diversity of technologies have been and still are being developed to extract the ocean wave energy for conversion into electricity. The most common devices are referred to as the Oscillating Water Column, hinged contour device, buoyant moored device, hinged flap, and overtopping device. The idea of integrating breakwater and OWC WEC emerged from an Indian wave energy program and has been discussed in Graw [21], which pointed out the advantage of shared costs between the breakwater and the wave energy device.

The OWC wave energy device basically consists of an air turbine installed at the upper outlet of a partially submerged chamber. The waves propagate into the chamber through the submerged lip wall opening. During the presence of a wave crest, the air column is pushed upwards through the duct and drives the turbine to generate electricity.

Conversely, when the wave troughs enter the chamber, the air column is pushed down. Hence, the pressure variations in the OWC chamber create a bidirectional air flow across the turbine, which rotates in a single direction for both flow directions (Fig. 1). This kind of turbine is therefore able to harness both flow directions. The efficiency of those self-rectifying turbines is however lower than the conventional unidirectional ones [22]. Some of the attractive properties of OWC devices are attributed to the use of an air turbine as machinery because it is the single moving part, it is not in contact with water, and provides an inherent energy storage by the inertia moment of the spinning shaft [23]. It should be noticed that the above-mentioned OWC-WECs are often based on shoreline or near-shore regions, which not only have the potential to harm the coastline environment but also are limited in terms of the deployment scale.

The first OWC device deployed into the sea on a large scale was in Japan [24]. After that, several OWC devices have been proposed and deployed. For example, a breakwater equipped with an OWC plant was finished with a 40 kW Wells turbine in the Sea of Japan [25]. Another plant was installed at the Pico Island (Azores, Portugal), equipped with a 400 kW horizontal-axis Wells turbine-generator set rated at 400 kW [26]. OWCs inserted in breakwaters can be installed in zones with low available energy [27], and some improvement in term of design are being investigated to enhance the device hydrodynamic performance. For instance, the U-OWC concept has been installed in a full operative plant in Italy in 2016 [28]. More recently, the benefit of the presence of two interconnected chambers and the installation of a proper dimensioned step in front of the device have been described in Rezanejad et al. [29] and Rezanejad et al. [30].

3. Exploitable wave energy assessment - methodology

The wave power density P is the rate at which the wave energy per unit length of wave crest is transmitted in the direction of wave propagation [31]:

$$P = \frac{1}{16}\rho g H_s^2 C_g \quad [1]$$

with ρ is the seawater density, g the gravitational acceleration, H_s the significant wave height defined as $Hs = 4\sqrt{m_0}$ with m_0 the area beneath the spectrum of the sea-state, and C_g the group velocity computed at the energy period.

In the present study, as the minimum water depth at the points of interest is about 30 m, most of the incoming wave periods fit into the intermediate water depth theory $(0.5 > h/L > 0,04)$, consequently the

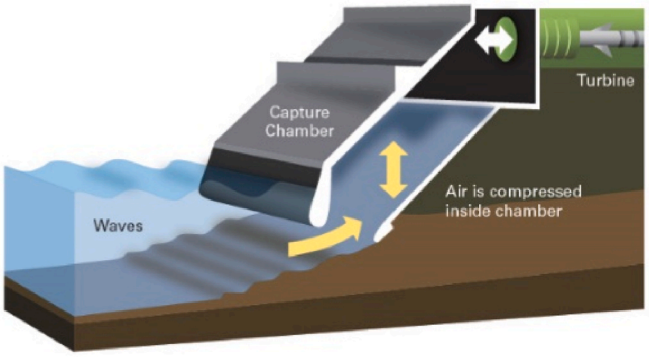

Fig. 1. Oscillating Water Column concept.

dispersion relation is implicit and the group velocity can be expressed as a function of the energy period as follows:

$$C_g = \frac{1}{2}\left[1 + \frac{2kh}{\sinh(2kh)}\right]\frac{L}{Te} \quad [2]$$

with *Te* the wave energy period and L the corresponding wavelength. For a thorough description of the concepts of energy period, significant wave height and group velocity see Cruz [32].

From Eqs. (1) and (2), the wave power density is given by:

$$P = \frac{\rho g H_s^2}{32}\left[1 + \frac{2kh}{\sinh(2kh)}\right]\frac{L}{Te} \quad [3]$$

The wavelength *L* is computed through the implicit dispersion relation: $\mu = kh = 2\pi h/L$ with *k*being the wave number and *h* the water depth. In his empirical work Beji [33] proposed an explicit approximate dispersion relation based on the explicit deep-water $(0.5 > h/L)$ dispersion relation, with an accuracy of 0.05% for the whole range of water depths:

$$\mu = kh = \mu_0\left[1 + \mu_0^{1.3} e^{-(1.1+2\mu_0)}\right]\frac{1}{\sqrt{\tanh\mu_0}} \quad [4]$$

With $\mu_0 = k_0 h = 2\pi h/L_0$, k_0 being the deep-water wave number and $L_0 = gT^2/2\pi$ the deep-water wavelength.

This equation has been implemented with success in Liang et al. [34], where they assess the accuracy of the wave energy calculation with the new approximate dispersion relation in deep water and shallow water conditions in the coastal water surrounding of Qingdao City (China). They compared the values obtained from the output of a validated third generation wave model and proved that the absolute average difference between both ways of computing wave energy is inferior to 15% in shallow and deep-water, improving the accuracy up to 300% compared with usual simplified wave energy assessment equation for shallow water.

Furthermore, the wave energy flux along a linear feature depends on the wave power density and on the angle between the wave direction and the axis of the structure hit by the waves. The wave energy flux across a linear feature is then given by Eq. (5), in which *P* is the incoming wave power density given by Eq. (3) and φ is the angle between the wave direction and the perpendicular to the breakwater pointing onshore:

$$P_\varphi = P\cos(\varphi) \quad [5]$$

Thus,

$$P_\varphi = \frac{\rho g H_s^2}{32}\left[1 + \frac{2kh}{\sinh(2kh)}\right]\frac{L}{Te}\cos(\varphi) \quad [6]$$

Negative values of the incoming wave power density can appear, and they stand for the reflected waves heading offshore. It is also necessary to consider the effect of the resource variability on performance. Non-linearities in device's hydrodynamics and the technological constraints of the electro-mechanical plant do imply a power level threshold above which the incoming energy is unexploitable, and such sea-states should be disregarded [35]. This threshold obviously depends on the device technology/design, so there is no definite value for it. Nowadays, the range of the overall average of wind-energy converter electric load factor, defined as the ratio of the average energy output over the highest possible electrical energy output on a specific time interval, is 25%–50%. It is a measure of the utilization rate, or efficiency of electrical energy usage; a high load factor indicates that the electric energy is being used efficiently. The maximum electrical energy (power level threshold) is defined as four times the average potential energy carried by the incoming waves [5]. As a consequence, a sea state producing more than the power level threshold should be discarded, because its energy will be above the electro-mechanical conversion capacity of the device. This new representation of the wave energy resource is called the exploitable wave energy resource since it is more closely related to the amount of wave energy exploitable by the WEC. Although this concept may provide a more rigorous estimation of the recoverable energy for wave energy converters, it is of paramount importance to carry out large scale tests with the selected device to refine the threshold value.

4. Modelling the nearshore wave climate

4.1. SWAN application

SWAN (version 43.31) is used in this paper to propagate the wave climate from offshore to nearshore. SWAN is a third-generation spectral wave model based on solving the spectral action balance equation, which determines the evolution of the action density in space and time [36]. The energy density is specified using the two-dimensional wave spectrum, with the wave energy distributed over frequency and propagation direction. Three regions were considered in this study (Fig. 2): Sines harbour area (a), Azores Central Group Islands (b) and Madeira Island (c). Various nested computational domains, embracing each zone of interest, were defined. Fig. 2 presents those computational domains as well as the locations of the available buoys whose measurements were used to check the goodness of the model predictions.

The implementation of the SWAN model was made for 36 equal direction ranges and 28 frequencies logarithmically spaced from 0.04 Hz to 0.6 Hz with a JONSWAP spectrum, the simulations being performed in the stationary mode, as it was found more effective from the computational point of view. A 40-year data hindcast was considered, from January 01, 1979 to July 31, 2019, to obtain a set of offshore wave estimates at the four borders of the main grids every 6 h. These estimates were extracted from the fifth generation ECMWF atmospheric reanalysis of the global climate, ERA5, and have been used to define the JONSWAP spectrum features at the main grid boundaries. The values of the forced inputs, for each simulation instant, are constant along each side of the main computational grid and correspond to the values extracted from the ERA5 reanalysis dataset at the midpoint of each side. The use of constant sea-wave characteristics can be justified by the low variation of the values along each side due to resolution constrains. The same reanalysed wind fields, also provided by the ERA5 dataset, are used as input for the model in all computational grids. It is defined to fit the main grid of each zone with a 0.25°/0.25° resolution every 6-h covering the whole 40-year time frame. The dimension and resolution of each grid is displayed in Table 1. The same wind field is used for every nested grids. According to previous works of Rusu & Guedes Soares [9] and Rusu et al. [37], current effects have no relevant impact on the sea waves of the 3 zones, so they were not considered, and refraction effects are only due to water depth variations. The default bottom friction coefficient proposed by the JONSWAP group (0.067 m^2s^{-3} [38], is used. This bottom friction coefficient has been found to be suitable for fully developed wave conditions in shallow water [39], although some variations will undoubtedly occur with different seabed conditions. The bathymetric data are extracted from EMODnet DTM resources. The physical processes activated in the SWAN simulations have been set by balancing the relevance of each factor in the studied area against its tendency to increase the calculation time (Table 2).

The physical processes not listed in Table 1 have been deactivated for the whole study. The Sines model only has one Nested grid and this grid has the same activated physical processes as in Nested 1 displayed in Table 1.

4.2. Nearshore wave climate modelling results

4.2.1. Result assessment

Three wave parameters are extracted from the numerical models –the significant wave height, the peak period, and the mean wave direction, defined in the SWAN code as follows:

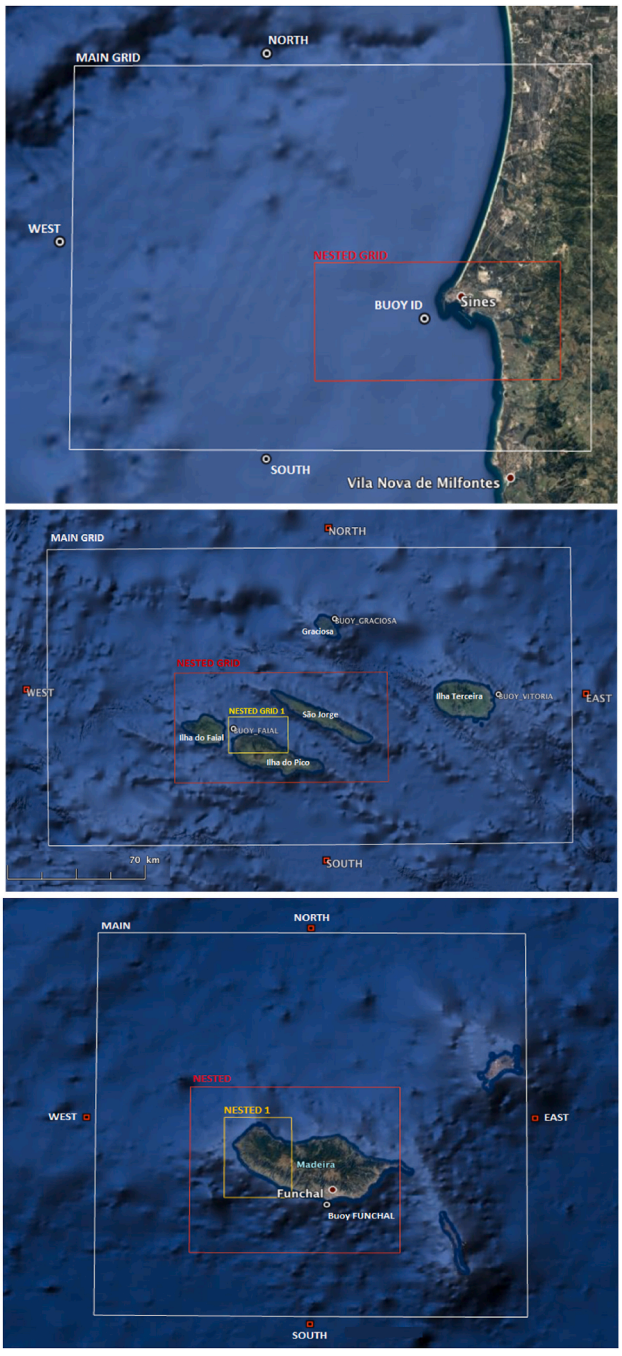

Fig. 2. Studied areas: a. Sines; b. Azores Central Group Islands (São Roque do Pico and Madalena do Pico); c. Madeira.

- Significant wave height (Hs) in m:

$$Hs = 4\sqrt{\iint E(\sigma,\theta)d\sigma d\theta} \quad [7]$$

With $E(\sigma,\theta)$ the energy density spectrum and σ the frequency (Hz) and θ the direction (rad).

- Relative peak period of E(ω) (Tpeak) in s – is the absolute maximum bin of the discrete wave spectrum and it is equal to the absolute peak period in absence of currents
- Mean wave direction (DIR) in ° - is the direction normal to the wave crests:

Table 1
Grids dimension and resolution – a. Sines b. Azores c. Madeira.

a. Grids	Dimension Lx (km)	Ly (km)	Resolution Δx (km)	Δy (km)
Main	71	53	0.49	0.49
Nested	35	17	0.098	0.098
b				
Main	265	149	1.2	1.2
Nested	106.8	54.6	0.6	0.6
Nested 1	30	18	0.1	0.1
c				
Main	138	135	1.2	1.2
Nested	69	60	0.6	0.6
Nested 1	29	18	0.1	0.1

$$DIR = \frac{180}{\pi} arctan\left(\frac{\int \sin\theta E(\sigma,\theta)d\sigma d\theta}{\int cos\ \theta E(\sigma,\theta)d\sigma d\theta}\right) \quad [8]$$

Those parameters are compared to in-situ measurements from buoys provided by the local harbours, to check if the corresponding wave model is introducing discrepancies. For that purpose, the following statistical parameters were considered (M - Model values & O - Observation values):

- the normalized Bias (NBias), describes the difference between the average of measurements made on a parameter and its simulated value; a value closer to zero characterizes a better simulation; values are over-predicted if NBias <0 and under-predicted if NBias >0:

$$NBias = \frac{\sum O - M}{\sum O} \quad [9]$$

- the normalized root mean square error (NRMSE):

$$NRMSE = \sqrt{\frac{\sum (M-O)^2}{\sum O^2}} \quad [10]$$

- the scatter index (SI) which gives the percentage of the expected error for the parameter:

$$SI = \sqrt{\frac{\sum ((M-\overline{M})-(O-\overline{O}))^2}{\sum O^2}} \quad [11]$$

- the linear correlation coefficient (r) which should be as close as possible to 1:

$$r = \frac{\sum (M-\overline{M})(O-\overline{O})}{\sqrt{\sum (O-\overline{O})^2 \sum (M-\overline{M})^2}} \quad [12]$$

- N – Number of values in the sample.

For the mean direction, the same statistical parameters have been computed using the circular statistics formulas [40]) in order to avoid the errors linked to the 360° modulus issues. The statistical comparisons are reported in Tables 3–5.

In general, H_s values are slightly overestimated, while T_p are underestimated. It is relevant to notice that the SI and the NRMSE, are similar to the values found through the ERA5 reanalysis dataset assessment performed in Anastas et al. [20], where data from ERA5 grid points close to the location of the buoys provided by the local harbours were compared to measurements from those buoys. Since ERA5 data

Table 2
Physical process activated in each grid of the SWAN model.

Physical Processes / GRIDS	Diffraction	Triad wave-wave interactions	Quadruplets wave-wave interactions	Bottom Friction	Depth-induced breaking	Wind	Tide
Main	ON	OFF	ON	OFF	ON	ON	ON
Nested	ON	ON	ON	OFF	ON	ON	ON
Nested 1	ON	ON	ON	ON	ON	ON	ON

Table 3
Sines - Statistical comparison of SWAN model and Buoy in-situ data from 2008 to 2018.

Parameters	NBias	NRMSE	SI	r	N
Hs	−0.1	0.21	0.19	0.92	7062
Tp	0.09	0.25	0.24	0.77	7062
Dir	0.06	0.07	0.06	0.74	7062

Table 4
Azores Central Group Islands - Statistical comparison of SWAN model and Buoy in-situ data from 2013 to 2019.

Parameters	NBias	NRMSE	SI	r	N
Hs	−0.19	0.29	0.27	0.86	6549
Tp	0.22	0.28	0.17	0.71	6549
Dir	0.092	0.061	0.13	0.87	6549

Table 5
Madeira - Statistical comparison of SWAN model and Buoy in-situ data from 1996 to 2002.

Parameters	NBias	NRMSE	SI	r	N
Hs	−0.26	0.21	0.19	0.83	882
Tp	0.43	0.25	0.24	0.61	882
Dir	0.03	0.35	0.06	0.98	882

from other grid points were used as input for the SWAN model, it can be concluded that sea-wave propagation with the SWAN model does not introduce almost any extra error comparing to sea-wave propagation in the ERA5 model. The high value of the NBias and the low value of the correlation coefficient for Tp at Madeira, can be explained by the bathymetric resolution or by the low number of accessible buoy data (N = 882).

4.2.2. Point of interest location

Since the aim of this paper is to assess the exploitable wave energy for OWC installation, one target point is selected in front of the breakwaters in each of the three zones, as close to the coast as the SWAN grid resolution allowed – Zone 1: Sines harbour West and East breakwater/ Zone 2: São Roque do Pico and Madalena do Pico/Zone 3: Paul do Mar (Fig. 3). The geographical coordinates of these points are listed in Table 6.

The extraction points, located, respectively, close to the Sines East and West breakwaters (Fig. 3a) are 40m away from the breakwater axis at a region where the water depth is about 30m. The elected spot for São Roque do Pico (Fig. 3b1) is about 30 m away from the breakwater axis at a region where the water depth is about 30m. For Madalena (Fig. 3b2) the closest site which allows modelling calculation is about 100m away from the breakwater axis, at a region where the water depth is about 35m. The point of interest for Paul do Mar (Fig. 3c) is about 50m away from the breakwater axis at a region where the water depth is about 40m. The consequence of using a one-direction projected definition of the wave power (see Eq. (5)) is that refraction will not significantly reduce the nearshore power resource because it will tend to narrow the directional dispersion of the incident waves on the perpendicular of the breakwater line. Thus, the energy calculated at the target points is considered a viable approximation of the energy available close to the breakwater.

4.2.3. Point of interest wave climate

Following the methodology described in section 3, two filters have been applied to the SWAN model results at each point of interest. After computing the exploitable energy flux from Eq. (6) every 6h over the 40 year-period (about 58000 values at each point for each parameter – Hs, Tp and Dir), the negative values were dismissed as well as their corresponding set of sea states, since they represent waves heading offshore. Then, the mean incident wave power was calculated for each point and used to determine the power level threshold, as defined in section 3, above which the values of wave power are excluded because considered as out of the range of the device hydro-mechanical conversion capacity (see Table 7). These filtered climate data series, coming from the five remaining target sites, are employed to generate wave roses and scatter diagrams of the $H_s - T_e$ joint distributions [41]). Such a diagram presents the occurrence probability of different sea states expressed as a percentage of the total number of occurrences and the colour of each bin indicates the percentage according to a colour-map, the same for all diagrams – dark red for high occurrences, yellow for intermediate and green for low occurrences. It is structured into bins of $2s \times 0.25m$ ($\Delta T_e \times \Delta H_s$). From those diagrams a global characterization of the sea-wave states can be obtained (Figs. 4–6 & Tables 8–10).

As expected, at such a small distance to the coast the direction distribution at each point is narrow and concentrated around the perpendicular of the breakwater axis. At Madalena and Sines West 80% of the occurrences are contained in a range of 6s in terms of energy period. The occurrence dispersion is significantly wider for the rest of the locations. Paul do Mar and São Roque do Pico exhibit a concentration of occurrences (>10%) at low values of Hs and Te, that will barely contribute to the power production. More details about those results are exposed further in part 4.2.5.

4.2.4. Point of interest exploitable wave power

The energy resources are now described by computing the mean recoverable energy flux, through Eq. (6), for each bin of the Hs–Te scatter diagram, whose resolution is 2s × 0.25m (ΔTe × ΔHs). The outcomes are presented in Tables 11–13.

The maximum and overall mean values of the energy flux are reported in Table 14.

Madalena and Sines W have the highest values of both maximum and overall mean energy flux. Nevertheless, no relevant conclusion can be drawn at this stage and the combination of the power bin diagrams and the occurrence diagrams is necessary to have a proper idea on the contribution of each bin (Hs–Te) in the energy production.

4.2.5. Point of interest exploitable wave energy

By multiplying the mean number of hours in one year (8766h) with the occurrence probability of each bin ($T_e - H_s$), in %, the annual occurrence probability of each bin in hour is obtained. The product of this occurrence (in hour) with the average exploitable power per wave front length (in kW/m) gives the average annual exploitable energy per unit wave crest length over the 40-year study in MWh/m [42]), as presented in Tables 15–17.

The largest contributions for the total annual mean recoverable energy come from sea states with both high occurrences and high wave

Fig. 3. Points of interest: a. Sines; b1. São Roque do Pico; b2. Madalena do Pico; c. Paul do Mar.

Table 6
Geographical coordinates of the extraction points.

	Sines W	Sines E	São Roque	Madalena	Paul do Mar
Geographical coordinates (ESPG)	37.94568°–8.890711°	37.935840°-8.862622°	38.5309986°–28.3186098°	38.5389778°-28.5321616°	32.751180°-17.224836°

Table 7
Threshold defined as four times the mean incident wave power in kW/m at each site.

	Sines W	Sines E	São Roque	Madalena	Paul do Mar
Threshold (kW/m)	110.1	45.4	33.3	63.5	27.7

power density (red bins). It suggests that WEC developers should design their devices in order to operate efficiently over sea conditions that provide the largest contributions to the total annual of wave energy, instead of aiming only the more common sea states that in general offer a small contribution to the overall exploitable energy.

- For the East breakwater of Sines port, the overall energy is about 5000MWyear/m. 80% of the exploitable energy contribution comes from sea states with significant wave heights between 0.5 and 2.25m and energy periods between 9s and 17s. It represents 68% of the sea state occurrences.
- For the West breakwater of Sines port, the overall energy is almost 20700MWyear/m. 80% of the exploitable energy contribution comes from sea states with significant wave heights between 1 and 3m and energy periods between 6s and 16s. It stands for 80% of the sea state occurrences.
- For São Roque do Pico, the overall energy is about 4900MWyear/m. 80% of the exploitable energy contribution comes from sea states with significant wave heights between 1m and 2.5m and energy periods between 6s and 14s. It represents 51% of the sea state occurrences.
- For Madalena, the overall energy is about 10500 MWyear/m. 80% of the exploitable energy contribution comes from sea states with significant wave heights between 0.75m and 3m and energy periods between 8 and 14s. It stands for 50% of the sea state occurrences.
- And finally, the overall energy is about 4040 MW year/m for Paul do Mar. 80% of the exploitable energy contribution comes from sea states with significant wave heights between 0.25m and 2m and

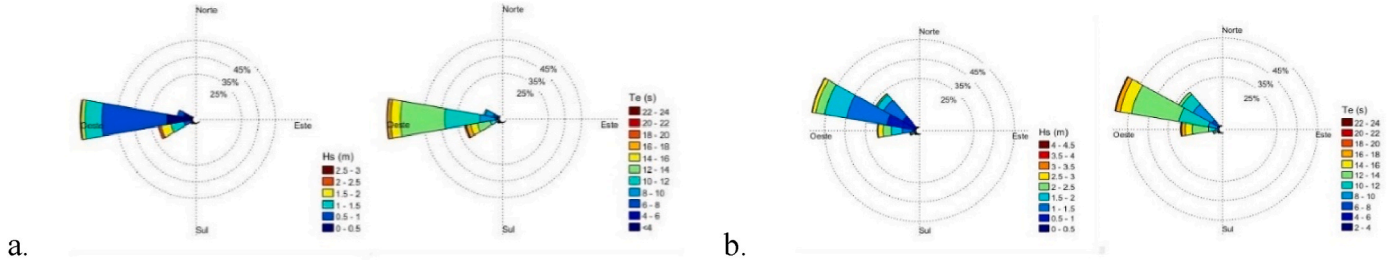

Fig. 4. Wave roses Hs-Dir and Te-Dir over the 40-year study period – a. Sines East; b. Sines West.

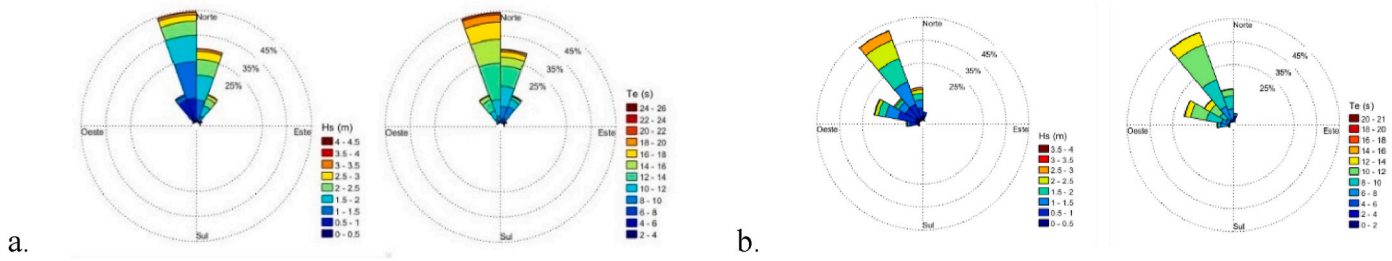

Fig. 5. Wave roses Hs-Dir and Te-Dir over the 40-year study period – a. São Roque do Pico; b. Madalena.

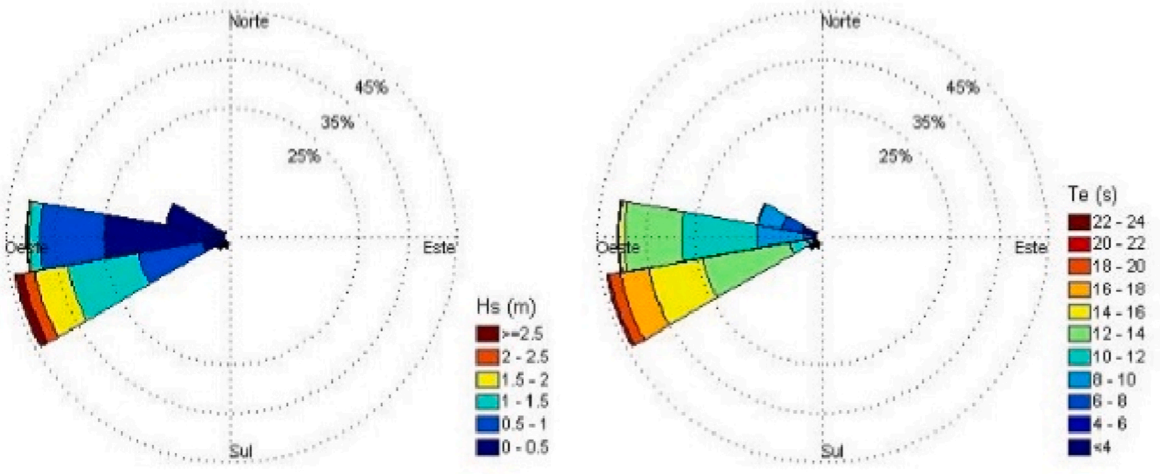

Fig. 6. Wave roses Hs-Dir and Te-Dir over the 40-year study period –Paul do Mar.

Table 8
Occurrence frequency diagram (in %) for each sea state over the 40-year study period – a. Sines East; b. Sines West..

a.

Hs (m) \ Te (s)	1	3	5	7	9	11	13	15	17	19	21	23
4	0	0	0	0	0	0	0	0	0	0	0	0
3.75	0	0	0	0	0	0	0	0	0	0	0	0
3.5	0	0	0	0	0	0	0	0	0	0	0	0
3.25	0	0	0	0	0	0	0	0	0	0	0	0
3	0	0	0	0.00	0	0	0	0	0	0	0	0
2.75	0	0	0	0.01	0	0.005	0.018	0.032	0.005	0	0	0
2.5	0	0	0.002	0.04	0.002	0.12	0.16	0.51	0.155	0.021	0.002	
2.25	0	0	0.01	0.09	0.07	0.39	0.45	1.09	0.18	0.029	0.002	
2	0	0	0.02	0.13	0.20	0.64	0.72	1.58	0.19	0.05	0.002	
1.75	0	0	0.06	0.14	0.42	1.06	1.14	1.99	0.18	0.05	0.01	
1.5	0	0.002	0.06	0.22	0.58	1.76	1.85	2.49	0.18	0.04	0.004	
1.25	0	0.01	0.10	0.41	0.90	3.40	3.23	3.08	0.19	0.04	0.004	
1	0	0.19	0.32	0.88	2.48	7.02	5.05	2.70	0.17	0.04	0.004	
0.75	0.04	0.66	0.63	2.47	7.11	12.38	3.44	1.56	0.09	0.02	0.01	
0.5	0.18	0.26	0.72	4.05	8.24	5.74	0.90	0.43	0.03	0.01	0.002	
0.25	0.10	0.01	0.04	0.42	0.79	0.24	0.03	0.01	0	0	0	

b.

Hs (m) \ Te (s)	0	2	4	6	8	10	12	14	16	18	20	22	24
4	0	0	0	0	0	0	0	0	0	0	0	0	0
3.75	0	0	0.002	0	0.009	0.014	0.010	0	0	0	0		
3.5	0	0	0.002	0	0.047	0.253	0	0.220	0.085	0.023	0.002		
3.25	0	0	0.002	0	0.13	0.44	0.36	0.363	0.115	0.028	0		
3	0	0	0.014	0.005	0.25	0.64	0.55	0.48	0.14	0.023	0		
2.75	0	0	0.045	0.07	0.36	1.08	0.76	0.58	0.10	0.02	0		
2.5	0	0	0.073	0.17	0.51	1.54	1.10	0.57	0.105	0.03	0.003		
2.25	0	0	0.160	0.40	0.81	2.44	1.35	0.61	0.103	0.03	0.002		
2	0	0.01	0.28	0.86	1.30	4.06	1.55	0.52	0.124	0.02	0.003		
1.75	0	0.10	0.54	1.40	2.21	5.79	1.39	0.46	0.122	0.02	0.005		
1.5	0	0.24	1.03	2.36	4.48	6.96	1.11	0.44	0.124	0.033	0.005		
1.25	0.009	0.344	1.66	4.37	6.81	5.91	0.86	0.32	0.101	0.02	0.005		
1	0.031	0.28	1.31	4.42	5.73	3.63	0.47	0.17	0.038	0.010	0.002		
0.75	0.042	0.14	0.56	2.69	2.57	1.26	0.18	0.07	0.017	0.007	0.002		
0.5	0.051	0.02	0.07	0.33	0.27	0.19	0.02	0.01	0.002	0.002	0		
0.25	0.005	0	0.002	0.005	0.002	0.002	0.002	0	0	0	0		

Table 9
Occurrence frequency diagram for each sea state (in %) over the 40-year study period – a. São Roque do Pico; b. Madalena..

a.

Hs (m) \ Te (s)	0	2	4	6	8	10	12	14	16	18	20	22
4	0	0	0	0	0	0	0	0	0	0	0	0
3.75	0	0	0	0	0	0	0	0	0	0	0	0
3.5	0	0	0	0	0.002	0	0	0	0	0	0	0
3.25	0	0	0	0	0.02	0.002	0	0	0	0	0	0
3	0	0	0.002	0.004	0.02	0.002	0	0	0	0	0	0
2.75	0	0	0.009	0.02	0.09	0.20	0.058	0.002	0	0	0	0
2.5	0	0	0.013	0.07	0.36	0.93	0.62	0.029	0	0	0	0
2.25	0	0	0.06	0.24	0.70	1.66	1.07	0.034	0	0	0	0
2	0	0.004	0.26	0.42	1.17	2.63	1.12	0.05	0.004	0	0	0
1.75	0	0.03	0.51	0.88	1.90	3.34	1.12	0.03	0	0	0	0
1.5	0	0.17	0.87	1.61	2.80	3.62	1.10	0.04	0	0	0	0
1.25	0	0.39	1.50	2.92	3.82	3.89	1.05	0.04	0.002	0	0	0
1	0	1.53	2.52	3.60	4.09	3.35	0.97	0.03	0.01	0	0	0
0.75	0	3.90	3.90	4.02	3.40	3.08	0.86	0.05	0.01	0.002	0	0
0.5	0.004	10.12	1.08	2.48	2.29	1.45	0.40	0.01	0	0.002	0.002	0
0.25	0.12	1.90	0.06	0.43	0.56	0.23	0.05	0.004	0.002	0	0	0

b.

Hs (m) \ Te (s)	0	2	4	6	8	10	12	14	16	18	20	22
4	0	0	0	0	0	0	0	0	0	0	0	0
3.75	0	0	0	0	0	0.004	0.002	0	0	0	0	0
3.5	0	0	0	0	0	0.004	0.01	0	0	0	0	0
3.25	0	0	0	0	0.06	0.39	0.33	0.016	0.004	0	0	0
3	0	0	0	0	0.27	1.42	1.14	0.11	0.002	0	0	0
2.75	0	0	0	0.02	0.61	2.06	1.28	0.07	0.007	0	0	0
2.5	0	0	0	0.10	1.21	2.76	1.30	0.09	0.002	0	0	0
2.25	0	0	0.004	0.24	1.87	3.31	1.27	0.07	0.004	0	0	0
2	0	0	0.02	0.67	2.84	3.56	1.23	0.05	0.002	0	0	0
1.75	0	0	0.06	1.47	3.51	3.55	1.25	0.06	0.005	0	0	0
1.5	0	0	0.18	2.45	3.79	3.49	1.20	0.05	0.005	0.004	0	0
1.25	0	0.002	0.50	3.52	3.77	3.53	1.11	0.06	0.011	0	0	0
1	0	0.07	0.89	4.27	4.13	3.57	1.15	0.09	0.012	0.002	0	0
0.75	0	0.69	1.18	4.05	4.03	2.75	0.87	0.05	0.005	0.004	0	0
0.5	0	1.83	0.41	2.52	2.57	1.09	0.28	0.04	0.007	0	0	0
0.25	0.01	0.45	0.04	0.50	0.38	0.05	0.04	0.01	0.005	0	0	0

Table 10
Occurrence frequency diagram for each sea state (in %) over the 40-year study period –Paul do Mar..

Hs (m) \ Te (s)	0	2	4	6	8	10	12	14	16	18	20	22	24
2.75	0	0	0	0	0	0	0	0	0	0	0	0	0
2.5	0	0	0	0	0	0	0	0	0	0	0	0	0
2.25	0	0	0	0	0.004	0.03	0.08	0	0	0	0.004	0	
2	0	0	0	0.01	0.08	0.20	0.60	0.60	0.87	0.49	0	0.016	
1.75	0	0	0	0.04	0.16	0.35	1.11	1.38	1.33	0.49	0.10	0.011	
1.5	0	0	0.03	0.12	0.23	0.56	2.29	2.53	1.42	0.33	0.06	0.004	
1.25	0	0.004	0.03	0.13	0.40	0.94	4.49	3.18	1.02	0.16	0.03	0.005	
1	0	0.03	0.02	0.19	0.58	1.87	6.55	2.26	0.60	0.13	0.03	0.009	
0.75	0	0.14	0.01	0.34	1.14	3.68	8.92	1.71	0.39	0.07	0.004	0.007	
0.5	0	1.58	0.03	1.85	7.70	10.20	6.39	0.68	0.16	0.04	0.007	0.002	
0.25	0.011	3.03	0.016	3.85	6.60	2.41	0.46	0.04	0.014	0.005	0	0	

energy periods between 10s and 18s. It represents 49% of the sea state occurrences.

The values are reported in Table 18 and can be used as indicators to choose the most suitable site for the OWC device installation.

4.2.6. Variability

Since the variability of the occurrences is also of a great importance in terms of design, in order to gather additional relevant information, three coefficients characterizing the variability of the wave power have been computed [43,44] and displayed in Table 18, namely:

- The coefficient of variation (COV), obtained by dividing the standard deviation of the power time series by the mean power The coefficient of variation for a fictitious power time series with absolutely no variability will be 0. This coefficient measures the variability at all-time scales.

$$COV(P) = \frac{\sigma(P(t))}{\mu(P(t))} \quad [13]$$

- The seasonal variability (SV) is used to capture in a single value a convenient measure of the seasonal variability of the wave energy resource. It is the difference between the mean wave power for the most energetic season (December to February) and for the least energetic season (June to August) divided by the mean annual power. It

Table 11
Mean exploitable energy flux per wave front length in kW/m for each sea state over the 40-year of study – a. Sines E; b. Sines W..

a.

Hs (m) \ Te (s)	0	1	3	5	7	9	11	13	15	17	19	21	23
3.25	0	0	0	0	0	0	0	0	0	0	0	0	
3	0	0	0	0	29.12	0	0	0	0	0	0	0	
2.75	0	0	0	0	29.35	0	44.10	42.44	44.16	45.17	0	0	
2.5	0	0	0	7.09	31.60	40.48	41.50	40.94	40.39	40.87	41.01	42.47	
2.25	0	0	0	6.15	21.87	41.20	36.22	33.42	32.79	33.89	34.46	36.51	
2	0	0	0	4.88	18.11	34.91	27.66	25.44	25.22	26.33	27.27	30.15	
1.75	0	0	0	3.81	16.52	30.49	19.99	18.67	18.65	19.26	19.73	23.41	
1.5	0	0	0.94	2.91	21.33	21.29	13.67	12.87	12.92	13.99	14.3127	14.21	
1.25	0	0	2.40	1.95	16.47	12.21	8.49	8.17	8.48	9.01	9.50	8.73	
1	0	0	0.80	0.95	7.45	6.34	4.76	4.84	5.10	5.58	5.28	6.13	
0.75	0	0.59	0.48	0.44	3.23	2.85	2.42	2.57	2.66	3.07	3.04	3.76	
0.5	0	0.25	0.21	0.12	1.30	1.25	1.05	1.09	1.10	1.18	1.18	0.98	
0.25	0	0.06	0.03	0.03	0.37	0.35	0.27	0.26	0.26	0	0	0	

b.

Hs (m) \ Te (s)	0	2	4	6	8	10	12	14	16	18	20	22	24
4	0	0	0	0	0	0	0	0	0	0	0	0	
3.75	0	0	95.35	0	100.90	107.49	108.61	0	0	0	0	0	
3.5	0	0	76.23	0	101.70	102.39	101.17	102.65	103.87	103.24	108.91		
3.25	0	0	47.71	0	92.31	88.05	88.16	88.98	90.40	89.32	0		
3	0	0	37.29	100.75	81.45	74.17	74.19	75.24	76.89	80.03	0		
2.75	0	0	40.69	99.31	67.57	61.53	61.37	62.42	63.63	65.47	0		
2.5	0	0	29.32	84.91	54.90	50.28	50.14	51.05	51.85	53.28	56.83		
2.25	0	0	19.84	71.86	43.64	39.82	40.14	40.75	41.52	41.09	48.83		
2	0	4.85	13.91	58.70	33.66	30.75	31.15	31.51	32.79	34.12	32.62		
1.75	0	4.63	9.18	44.71	24.93	22.96	23.61	23.84	24.06	25.91	25.59		
1.5	0	4.21	6.90	31.39	17.48	16.47	16.78	17.30	17.57	17.65	13.82		
1.25	6.33	2.26	4.39	21.09	12.11	11.16	11.35	11.50	11.95	11.88	12.08		
1	2.49	1.41	3.10	13.56	7.52	6.92	6.72	7.02	6.69	7.17	7.62		
0.75	0.55	0.91	1.91	7.39	4.15	3.64	3.75	3.72	3.94	3.40	2.83		
0.5	0.16	0.54	0.86	3.34	1.78	1.39	1.12	1.71	2.11	1.37	0		
0.25	0.065	0	0.08	0.50	0.06	0.56	0.43	0	0	0	0		

Table 12
Mean exploitable energy flux per wave front length in kW/m for each sea state over the 40-year of study – a. São Roque do Pico; b. Madalena..

a.

Hs (m) \ Te (s)	0	2	4	6	8	10	12	14	16	18	20	22
4	0	0	0	0	0	0	0	0	0	0	0	0
3.75	0	0	0	0	0	0	0	0	0	0	0	0
3.5	0	0	0	0	31.76	0	0	0	0	0	0	0
3.25	0	0	0	0	29.62	29.01	0	0	0	0	0	0
3	0	0	25.91	26.36	25.47	33.10	0	0	0	0	0	0
2.75	0	0	22.16	28.05	26.56	30.70	31.80	32.83	0	0	0	0
2.5	0	0	11.42	23.67	27.19	28.42	29.86	30.05	0	0	0	0
2.25	0	0	14.50	21.83	22.53	23.45	24.80	26.00	0	0	0	0
2	0	6.23	8.80	19.41	17.40	18.04	18.94	19.29	20.00	0	0	0
1.75	0	4.48	5.66	15.99	12.99	13.51	14.03	15.36	0	0	0	0
1.5	0	2.96	4.29	12.42	9.31	9.47	9.86	10.61	0	0	0	0
1.25	0	6.12	2.97	8.08	6.09	6.12	6.36	7.48	7.51	0	0	0
1	0	6.88	1.54	4.89	3.59	3.55	3.89	4.12	4.50	0	0	0
0.75	0	2.02	0.56	2.62	1.80	1.80	2.03	2.08	1.81	2.65	0	
0.5	0.07	1.03	0.29	1.03	0.71	0.76	0.83	0.74	0	1.61	1.53	
0.25	0.01	0.07	0.11	0.21	0.16	0.15	0.15	0.09	0.16	0	0	

b.

Hs (m) \ Te (s)	0	2	4	6	8	10	12	14	16	18	20	22
4	0	0	0	0	0	0	0	0	0	0	0	0
3.75	0	0	0	0	0	47.19	52.45	0	0	0	0	0
3.5	0	0	0	0	0.00	44.07	46.63	0	0	0	0	0
3.25	0	0	0	0	61.17	59.81	60.58	57.08	63.03	0	0	0
3	0	0	0	0	53.33	52.34	53.91	55.70	55.06	0	0	0
2.75	0	0	0	55.01	44.12	43.68	44.87	45.53	48.05	0	0	0
2.5	0	0	0	40.49	34.96	35.65	36.54	36.71	40.03	0	0	0
2.25	0	0	43.24	33.39	27.53	28.36	28.77	28.85	28.50	0	0	0
2	0	0	30.81	27.21	21.70	22.05	22.28	22.12	24.81	0	0	0
1.75	0	0	18.76	21.23	16.55	16.25	16.51	16.36	12.88	0	0	0
1.5	0	0	11.93	15.35	11.76	11.33	11.43	11.57	13.01	12.20	0	0
1.25	0	1.849	6.792	10.50	7.80	7.33	7.40	7.44	7.73	0	0	0
1	0	3.316	3.319	6.47	4.49	4.37	4.43	4.50	4.71	5.52	0	0
0.75	0	4.214	1.635	3.19	2.28	2.33	2.34	2.20	1.84	2.31	0	0
0.5	0	0.908	0.543	1.19	0.90	0.94	0.91	0.93	0.99	0	0	0
0.25	0.003	0.04	0.26	0.28	0.25	0.19	0.22	0.17	0.25	0	0	0

Table 13
Mean exploitable energy flux per wave front length in kW/m for each sea state over the 40-year of study – Paul do Mar..

Table 14
Maximum and overall mean exploitable energy flux per wave front length in kW/m at each site.

	Sines E	Sines W	São Roque	Madalena	Paul do Mar
Maximum (kW/m)	45.2	108.9	33.1	63.0	28
Overall (kW/m)	14.95	35.8	11.1	20.4	9.6

quantifies the variability on a 3-month seasonal time scale and it is not influenced by variability at shorter time scales.

$$SV = \frac{P_{smax} - P_{smin}}{P_{year}} \quad [14]$$

➢ And finally, the inter-annual variability (IAV) defined as the standard deviation of the mean values of each year normalized by the overall mean. It only quantifies the variability on a 12-month scale (October–September).

$$IAV = \frac{\sigma_{\mu(P(t))}}{\mu(P(t))} \quad [15]$$

Table 17
Mean exploitable energy per wave front length in MWyear/m – São Paul do Mar..

Table 18
Indicators for OWC device installation at potential sites.

	São Roque	Madalena	Sines West	Sines East	Paul do Mar
Distance from the breakwater (m)	30	100	50	50	50
Water Depth	30	35	30	30	40
Hsmax (m)	11.3	4.1	7.5	6.8	6.4
Coefficient of variation	1.35	0.97	1.11	1.75	1.83
Seasonal Variability	0.84	0.92	0.84	1.4	1.63
Inter-Annual Variability	3.7%	2.2%	3.0%	4.6%	3.7%
Threshold Value (kW/m)	33.3	63.5	110.1	45.3	27.7
Values Over Threshold	4.2%	1.7%	2.8%	5.2%	4.7%
Exploitable Mean Annual Energy (Mwyear/m^{-1})	5742	13023	20753	6185	4041
80% Mean annual energy Occurrences (%)	51%	50%	80%	68%	49%
Te range	6s–14s	8s–14s	8s–16s	9s–17s	10s–18s

Table 15
Mean exploitable energy per wave front length in MWyear/m – a. Sines E; b. Sines W..

a.
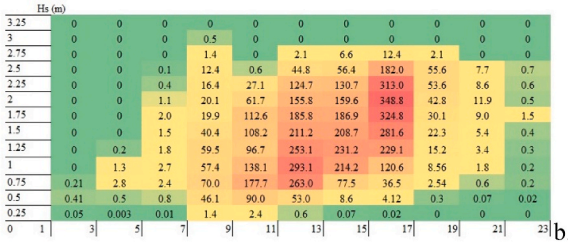

b.
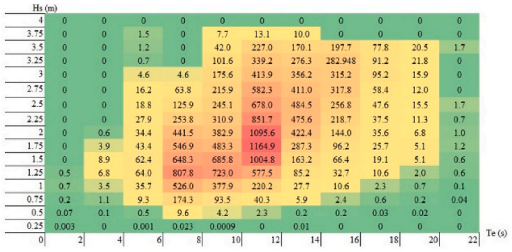

Table 16
Mean exploitable energy per wave front length in MWyear/m – a. São Roque do Pico; b. Madalena..

a.


b.


5. OWC device installation site selection

Table 18 summarizes the results for each potential site for the 40-year study period to compare their relative relevancy for the installation of an OWC device.

The second row shows the water depth at each point of interest. The third row displays the maximum values of significant wave height before applying the threshold filter. It comes as a pertinent information when designing the device because the turbine shouldn't be in contact with the water so the higher are the incoming waves the higher should be the air chamber.

The next three lines indicate the variability of the exploitable energy for 3 different period scales – hourly, seasonally, and annually. Low variability means that the sea states are more predictable and that the design of the device would be eased. The next two lines indicate the power level threshold values and the percentage of power values that had been discarded, because considered as out of range of the device conversion capacity. It gives an idea of the quantity of strong events that the structure would endure as well as the fraction of sea states whose energy cannot be converted because of technology limitation. Thus, this value should be as low as possible. The eighth row shows the overall mean annual energy in MWyear/m. It represents the amount of energy that is potentially available in front of each OWC device. And finally, the last row shows the contribution of the sea state occurrences and the range of energy period that produce 80% of the overall mean energy. Low contribution values indicate that the sea states with high occurrences coincides with the sea states of high wave power density. Therefore, most of the energy can be gathered from a small number of incoming sea states. Concerning the energy period range that produces those 80%, the thinner this range is the easier it would be to design the device and to tune its eigen periods to the dominant incoming wave period range.

Thus, from the point of view of the amount of energy available Sines West is the most appropriate site as it has higher exploitable mean annual energy. Considering the wave state variability and predictability, Madalena's breakwater appears to be the most suitable place for OWC installation as is shows lower variability for all time scales. It is as well the best alternative when it comes to design complexity as it presents lower Hsmax and less values over the threshold and a narrow wave energy period range to produce 80% of the overall mean annual energy available. It is also the second choice regarding the overall mean annual energy. Given all those factors, it has been decided that best location in terms of energy conversion and design complexity is Madalena Harbour on the Pico Island.

6. Conclusions

A third-generation spectral wave model, together with hindcast data from the ERA5 reanalysis dataset, has been set-up to investigate the energetic potential of five selected locations. Because of the large temporal scale of the study (40 years), it should be born in mind that some choices in term of modelling had to be made by balancing the calculation time against the impact of each factor on the study's accuracy. For instance, the activated parameters in each grid, the computational grid resolutions, the stationary mode, and the forced input data at the middle of each of the 4 sides the coarsest computational domain instead of continuous spectral inputs at the same sides. All these simplifications introduce non-negligible errors. Nevertheless, the model accuracy has been confirmed thanks to in-situ buoy measurement and the amount of information produced by such a study gives a rigorous overview of the general tendencies. The concept of exploitable wave energy resource was considered in this study since it provides a more appropriate representation in the context of a non-axisymmetric wave energy converter. It was observed that, in order to reach the highest efficiency, the greatest values of occurrences should be associated to the high-power sea state. Furthermore, the energy period range of the highest values of occurrences should be as small as possible, making the design of an effective converter, regarding its eigen-periods, eased by the narrower range of wave energy period that the device should be able to convert.

CRediT authorship contribution statement

Gael Anastas: Conceptualization, Methodology, Writing – original draft. **João Alfredo Santos:** Visualization, Supervision, Writing-Reviewing. **C.J.E.M. Fortes:** Supervision, reviewing. **Liliana V. Pinheiro:** reviewing.

Declaration of competing interest

The authors declare that they have no known competing financial interests or personal relationships that could have appeared to influence the work reported in this paper.

Acknowledgement

This work has been performed within the projects OWC-HARBOUR - Harbour protection with dual chamber oscillating water column devices (PTDC/EME-REN/30866/2017) and To-SEAlert - Wave overtopping and flooding in coastal and port areas: Tools for an early warning, emergency planning and risk management system (PTDC/EAM-OCE/31207/2017), funded by the Portuguese Foundation for Science and Technology.

References

[1] A. Clément, P. McCullen, A. Falcão, A. Fiorentino, F. Gardner, K. Hammarlund, G. Lemonis, T. Lewis, K. Nielsen, S. Petroncini, M.T. Pontes, P. Schild, B. O. Sjöström, H.C. Sørensen, T. Thorpe, Wave energy in Europe: current status and perspectives, Renew. Sustain. Energy Rev. 6 (Issue 5) (2002), https://doi.org/10.1016/S1364-0321(02)00009-6.

[2] B. Drew, A.R. Plummer, M.N. Sahinkaya, A Review of Wave Energy Converter Technology Department of Mechanical Engineering, University of Bath, Bath, UK, 2009, https://doi.org/10.1243/09576509JPE782.

[3] A.F. Falcão, Wave energy utilization: a review of the technologies, Renew. Sustain. Energy Rev. 14 (3) (2010) 899–918, 2010.

[4] J. Falnes, A review of wave-energy extraction, Mar. Struct. 20 (2007) (2007) 185–201, https://doi.org/10.1016/j.marstruc.2007.09.001.

[5] M. Folley, T.J.T. Whittaker, Analysis of the nearshore wave energy resource, Renew. Energy 34 (2009) 7 1709–1715.

[6] Electric Power Research Institute, Mapping and Assessment of the United States Ocean Wave Energy Resource, 2011. Technical report.

[7] E. Rusu, P. Pilar, C. Guedes Soares, Evaluation of the wave conditions in Madeira Archipelago with spectral models, Ocean Eng. 35 (2008) 1357e71.

[8] A. Matos, F. Madeira, C.J.E.M. Fortes, E. Didier, P. Poseiro, J. Jacob, Wave energy at Azores islands, in: SCACR2015 – International Short Course/Conference on Applied Coastal Research, 28th Sep. – 1st Oct. 2015 – Florence, Italy, 2015, pp. 243–254. ISBN 78-88-97181-52-1.

[9] L. Rusu, C. Guedes Soares, Wave energy assessments in the Azores islands, Renew. Energy 45 (2012) 183–196.

[10] E. Rusu, C. Guedes Soares, Numerical modelling to estimate the spatial distribution of the wave energy in the Portuguese nearshore, Renew. Energy 34 (Issue 6) (2009) 1501–1516. June 2009.

[11] P. Mota, J.P. Pinto, Wave energy potential along the western Portuguese coast, Renew. Energy 71 (November 2014) (2014) 8–17.

[12] E. Rusu, Evaluation of the wave energy conversion efficiency in various coastal environments, Energies 7 (2014) 4002–4018, https://doi.org/10.3390/en7064002.

[13] G. Iglesias, R. Carballo, Wave power for La Isla Bonita, Energy 35 (12) (2010).

[14] A.R. Bento, P. Martinho, C. Guedes Soares, Modelling wave energy for the north coast of Spain, in: Maritime Engineering and Technology - Proceedings of 1st International Conference on Maritime Technology and Engineering, 2012, https://doi.org/10.1201/b12726-79. MARTECH 2011.

[15] M. Monteforte, C. lo Re, G.B. Ferreri, Wave energy assessment in Sicily (Italy), Renew. Energy 78 (2015), https://doi.org/10.1016/j.renene.2015.01.006.

[16] M. Gonçalves, P. Martinho, C. Guedes Soares, Wave energy assessment based on a 33-year hindcast for the Canary Islands, Renew. Energy 152 (June 2020) (2020) 259–269.

[17] S. Ahn, K.A. Haas, V.S. Nearyb, Wave energy resource characterization and assessment for coastal waters of the United States, Appl. Energy 267 (1 June 2020) (2020), 114922.

[18] A. Ribal, A.V. Babanin, S. Zieger, Q. Liu, A high-resolution wave energy resource assessment of Indonesia, Renew. Energy 160 (November 2020) (2020) 1349–1363.

[19] R.P. Patel, K. Galarpati, S.S. Kachhwaha, S.V.V. Arun Kumar, M. Seemanth, Combined wind and wave resource assessment and energy extraction along the Indian coast, Renew. Energy 195 (August 2022) (2022) 931–945.
[20] G. Anastas, J.A. Santos, L.V. Pinheiro, C.J.E.M. Fortes, Wave energy assessment in the Azores Island for OWC installation, in: MARETECH 2020 Conference, Lisbon, IST, vol. 2, Renewable Energy, 2019, p. 511.
[21] K.-U. Graw, Wave energy breakwaters - a device comparison, in: Conference in Ocean Engineering, IIT Madras, India, 1996.
[22] A.F. Falcão, J.C. Henriques, L.M. Gato, Self-rectifying air turbines for wave energy conversion: a comparative analysis, Renew. Sustain. Energy Rev. 91 (2018) (2018) 1231–1241.
[23] T.V. Heath, A review of oscillating water columns, Phil. Trans. 370 (2012) 235–245.
[24] A.F. Falcão, J.C.C. Henriques, Oscillating-water-column wave energy converters and air turbines: a review, Renew. Energy 85 (2016) (2016) 1391–1424.
[25] Y. Masuda, M.E. Mccormick, Experiences in pneumatic wave energy conversion in Japan, in: Utilization of Ocean Waves Wave to Energy Conversion, ASCE Library, Reston, VA, USA, 2015, pp. 1–33.
[26] A.F. Falcão, A.J.N.A. Sarmento, L.M.C. Gato, A. Brito-Melo, The Pico OWC wave power plant: its lifetime from conception to closure 1986–2018, Appl. Ocean Res. 98 (2020), 102104, https://doi.org/10.1016/J.APOR.2020.102104.
[27] S. Naty, A. Viviano, E. Foti, Wave energy exploitation system integrated in the coastal structure of a mediterranean port, Sustainability 8 (2016) 12.
[28] F. Arena, A. Romolo, G. Malara, V. Fiamma, V. Laface, The first full operative U-OWC plants in the port of Civitavecchia, in: Proceedings of the International Conference on Offshore Mechanics and Arctic Engineering - OMAE, vol. 10, 2017, https://doi.org/10.1115/OMAE2017-62036.
[29] K. Rezanejad, J. Bhattacharjee, C. Guedes Soares, Analytical and numerical study of dual-chamber oscillating water columns on stepped bottom, Renew. Energy 75 (2015) 272–282, https://doi.org/10.1016/j.renene.2014.09.050.
[30] K. Rezanejad, J.F.M. Gadelho, I. López, R. Carballo, C. Guedes Soares, Improving the hydrodynamic performance of owc wave energy converter by attaching a step, in: Proceedings of the International Conference on Offshore Mechanics and Arctic Engineering - OMAE vol. 10, 2019, https://doi.org/10.1115/omae2019-96408.
[31] R.G. Dean, R.A. Dalrymple, Water Wave Mechanics for Engineers and Scientists, 1991. ISBN: 0-13-946038-1.
[32] J. Cruz, Ocean Wave Energy, Springer, Berlin Heidelberg, 2008 (Chapter 4).2.
[33] S. Beji, Improved explicit approximation of linear dispersion relationship for gravity waves, Coast. Eng. 73 (March 2013) (2013) 11–12. Short communication.
[34] B. Liang, Z. Shao, G. Wu, M. Shao, J. Sun, New equations of wave energy assessment accounting for the water depth, Appl. Energy 188 (15 February 2017) (2017) 130–139.
[35] B. Cahill, A.W. Lewis, Wave energy resource characterization of the Atlantic marine energy test site, in: Proceedings of the 9th European Wave and Tidal Energy Conference, Southampton, UK, 2011.
[36] N. Booij, R. Ris, L. Holthuijsen, A third-generation wave model for coastal regions, Part I, Model description and validation, J. Geophys. Res. 104 (C4) (1999) 7649–7666.
[37] E. Rusu, P. Pilar, C. Guedes Soares, Hindcast of the wave conditions along the west Iberian coast, Coast. Eng. 55 (2008) 906e19.
[38] K. Hasselmann, T.P. Barnett, E. Bouws, H. Carlson, D.E. Cartwright, K. Enke, J. A. Ewing, H. Gienapp, D.E. Hasselmann, P. Kruseman, A. Meerburg, P. Mller, D. J. Olbers, K. Richter, W. Sell, H. Walden, Measurements of wind-wave growth and swell decay during the joint north sea wave project (JONSWAP), Ergnzungsheft zur Deutschen Hydrographischen Zeitschrift Reihe A (8) (1973) 95. Nr. 12, 1973.
[39] E. Bouws, G.J. Komen, On the balance between growth and dissipation in an extreme depth-limited wind-sea in the southern North Sea, J. Phys. Oceanogr. 13 (9) (1983) 1653–1658.
[40] R.J. Yamartino, A Comparison of Several “Single-Pass” Estimators of the Standard Deviation of Wind Direction, Environmental Research and Technology, Inc., Concord, MA 0142, 1984.
[41] D. Silva, E. Rusu, C. Guedes Soares, Evaluation of various technologies for wave energy conversion in the Portuguese nearshore, Energies 6 (3) (2013) 1344–1364.
[42] D. Dunnett, J.S. Wallace, Electricity generation from wave power in Canada, Renew. Energy 34 (1) (2009) 179–195. January 2009.
[43] A.M. Cornett, A global wave energy resource assessment, in: Proceedings of the Eighteenth International Offshore and Polar Engineering Conference (ISOPE), International Society of Offshore and Polar Engineers, Vancouver, 6–11 July 2008, 2008. Paper No. ISOPE-2008-579.
[44] B.G. Reguero, I.J. Losada, F.J. Méndez, A global wave power resource and its seasonal, interannual and long-term variability, Appl. Energy 148 (2015) (2015) 366–380, https://doi.org/10.1016/j.apenergy.2015.03.114.